more, the organization of these fossils, taken together with their provenance, indicates that the genetic tool kit and pattern formation mechanisms required for bilaterian development had already evolved by Doushantuo times, long before the Cambrian. Therefore, the diversification of body plans in the Early Cambrian followed from the varied deployment of these mechanisms once conditions permitted, not from their sudden appearance at or just before the Cambrian boundary.

References and Notes

1. J. Y. Chen, G. Zhou, in *The Cambrian Explosion and the Fossil Record*, J. Y. Chen, Y-N. Cheng, H. V. Iten, Eds. (Bulletin of the National Museum of Natural Science, Taiwan, 1997), Vol. 10, pp. 11–116.
2. M. A. Fedonkin, B. M. Waggoner, *Nature* **388**, 868 (1997).
3. M. W. Martin *et al.*, *Science* **288**, 841 (2000).
4. A. H. Knoll, *Life on a Young Planet: The First Three Billion Years of Evolution on Earth* (Princeton University Press, Princeton, NJ, 2003).
5. J. P. Grotzinger, S. A. Bowring, B. Z. Saylor, A. J. Kaufman, *Science* **270**, 598 (1995).
6. K. J. Peterson *et al.*, *Proc. Natl. Acad. Sci. U.S.A.* **101**, 6536 (2004).
7. P. F. Hoffman, A. J. Kaufman, G. P. Halverson, D. P. Schrag, *Science* **281**, 1342 (1998).
8. W. T. Hyde, T. J. Crowley, S. K. Baum, W. R. Peltier, *Nature* **405**, 425 (2000).
9. B. Runnegar, *Nature* **405**, 403 (2000).
10. D. H. Erwin, E. H. Davidson, *Development* **129**, 3021 (2002).
11. E. H. Davidson, *Genomic Regulatory Systems: Development and Evolution* (Academic Press, San Diego, CA, 2001).
12. G. H. Barfod *et al.*, *Earth Planet. Sci. Lett.* **201**, 203 (2002) (*31*).
13. S. Xiao, A. H. Knoll, *J. Paleontol.* **74**, 767 (2000).
14. S. Xiao, X. Yuan, A. H. Knoll, *Proc. Natl. Acad. Sci. U.S.A.* **97**, 13684 (2000).
15. J.-Y. Chen *et al.*, *Proc. Natl. Acad. Sci. U.S.A.* **97**, 4457 (2000).
16. J.-Y. Chen *et al.*, *Dev. Biol.* **248**, 182 (2002).
17. Y. Zhang, L. M. Yin, S. H. Xiao, A. H. Knoll, *Paleontol. Soc. Mem.* **50**, 1 (1998).
18. X. L. Yuan *et al.*, *Doushantuo Fossils: Life on the Eve of Animal Radiation* (University of Science and Technology of China Press, Hefei, 2002), pp. 1–171.
19. D. F. Chen, W. Q. Dong, L. Qi, G. Q. Chen, X. P. Chen, *Chem. Geol.* **201**, 103 (2003).
20. H. Kimura *et al.*, *GSA Abstr. Prog.* **35**, Abstr. 187-11 (2003).
21. Z. Zhao *et al.*, *China Univ. Geol. Press*, pp. 1–205 (1988).
22. S. Q. Dornbos, D. J. Bottjer, *GSA Abstr. Prog.* **34**, Abstr. 75-6 (2002).
23. F. Gao *et al.*, *GSA Abstr. Prog.* **35**, Abstr. 187-10 (2003).
24. Systematic paleontology of *Vernanimalcula* is available on *Science* Online.
25. R. C. Brusca, G. J. Brusca, *Invertebrates* (Sinauer Associates, Sunderland, MA, ed. 2, 2003).
26. A. M. Ruiz-Trillo, M. Riutort, D. T. J. Littlewood, E. A. Herniou, J. Baguna, *Science* **283**, 1919 (1999).
27. U. Jondelius, I. Ruiz-Trillo, J. Baguna, M. Riutort, *Zool. Scr.* **31**, 201 (2002).
28. J. Baguna *et al.*, *Int. J. Dev. Biol.* **45**, S133 (2001).
29. A. M. A. Aguinaldo *et al.*, *Nature* **387**, 489 (1997).
30. K. M. Halanych *et al.*, *Science* **267**, 1642 (1995).
31. This analysis yielded a Lu-Hf age of 584 +/– 26 Ma and a Pb-Pb age of 599.3 +/– 4.2 Ma.

32. This research was supported by National Science Foundation of China Grant 40132010, National Department of Science and Technology Grant 2000077700, and National Laboratory of Paleontology and Stratigraphy Grant 033115 (J.-Y.C.), the National Science Council of Taiwan (C.-W.L.), and NASA/Ames Grant NAG2-1541 (E.H.D.). P.O. was supported by the Camilla Chandler Frost Fellowship.

Supporting Online Material

www.sciencemag.org/cgi/content/full/1099213/DC1
SOM Text

16 April 2004; accepted 21 May 2004
Published online 3 June 2004;
10.1126/science.1099213
Include this information when citing this paper.

The Bacterial Condensin MukBEF Compacts DNA into a Repetitive, Stable Structure

Ryan B. Case,[1,2*] Yun-Pei Chang,[3*] Steven B. Smith,[2,4] Jeff Gore,[2] Nicholas R. Cozzarelli,[1,3†] Carlos Bustamante[1,2,3,4†]

Condensins are conserved proteins containing SMC (structural maintenance of chromosomes) moieties that organize and compact chromosomes in an unknown mechanism essential for faithful chromosome partitioning. We show that MukBEF, the condensin in *Escherichia coli*, cooperatively compacts a single DNA molecule into a filament with an ordered, repetitive structure in an adenosine triphosphate (ATP) binding–dependent manner. When stretched to a tension of ~17 piconewtons, the filament extended in a series of repetitive transitions in a broad distribution centered on 45 nanometers. A filament so extended and held at a lower force recondensed in steps of 35 nanometers or its multiples; this cycle was repeatable even in the absence of ATP and free MukBEF. Remarkably, the pattern of transitions displayed by a given filament during the initial extension was identical in every subsequent extension. Hence, after being deformed micrometers in length, each filament returned to its original compact structure without the addition of energy. Incubation with topoisomerase I increased the rate of recondensation and allowed the structure to extend and reform almost reversibly, indicating that supercoiled DNA is trapped in the condensed structure. We suggest a new model for how MukBEF organizes the bacterial chromosome in vivo.

Chromosomes must be organized into compact structures to be correctly segregated into daughter cells. Whereas the first levels of chromosome structure have been well described [e.g., folding of DNA into nucleosomes in eukaryotes (*1*)], higher orders of DNA compaction are still not understood. Proteins that play a critical role in the organization and higher order folding of mitotic chromosomes and bacterial nucleoids are members of the SMC family called condensins (*2*–*5*).

Condensins consist of an SMC dimer and non-SMC subunits. Each SMC protomer contains, in order, an N-terminal globular domain with a Walker-A consensus sequence, a long α helix, a hinge domain, a second long α helix, and a C-terminal globular region having both a Walker-B box and an ATP-binding cassette (ABC) signature motif. This polypeptide folds back onto itself to form an antiparallel coiled coil, with the hinge at one end and a globular head domain containing the DNA and ATP-binding regions at the other end (*6*). A partial structure of the SMC protein Rad50 shows that two globular heads come together in trans to form two ATP-binding pockets and a potential DNA binding groove (*7*). Folded SMC protomers dimerize through interactions of the hinges and then associate with two or three non-SMC factors. A complete condensin typically has a molecular mass of ~600 kD (*8*). This overall architecture is conserved among diverse organisms, which suggests that it is important for function in vivo.

Despite the multiple vital roles of SMC proteins in the cell, very little is known about the molecular mechanisms by which they act. One of the best characterized SMC proteins, 13*S* condensin from *Xenopus laevis*, localizes to a central axis along the length of in vitro–assembled *Xenopus* mitotic chromosomes (*9*). It is required for the initiation and maintenance of mitotic chromosome condensation (*10*), introduces global positive writhe into naked DNA in the presence of ATP (*11*), and is a weak DNA-stimulated ATPase (*12*). Condensins with similar functions and activities have also been described in yeast (*13*, *14*), worms (*15*), and bacteria (*16*, *17*).

The *E. coli* condensin, MukBEF, consists of MukB (the SMC subunit) and MukE and MukF (*8*, *17*). Mutational inactivation of any of the

[1]Department of Molecular and Cell Biology, [2]Department of Physics, [3]Biophysics Graduate Group, [4]Howard Hughes Medical Institute, University of California, Berkeley, CA 94720, USA.

*These authors contributed equally to this work.
†To whom correspondence should be addressed. E-mail: ncozzare@socrates.berkeley.edu (N.R.C.), carlos@alice.berkeley.edu (C.B.)

three *muk* genes results in a factor of 100 increase in anucleate cell formation, temperature-sensitive growth, and expanded and disordered nucleoids (*17*, *18*). A mutation in the topoisomerase I gene suppresses the Muk phenotype, probably because the absence of this topoisomerase leads to an increased compaction of the nucleoid by the additional negative supercoils (*19*). MukBEF localizes to the center of the nucleoid (*20*), reminiscent of the central chromosomal localization of 13*S* condensin. Therefore, MukBEF, like eukaryotic condensins, maintains a compacted state of the chromosome that is required for appropriate segregation.

But how do condensins compact and organize DNA? Condensins are probably not molecular motors that use the energy of ATP hydrolysis to reel in DNA. The structures of the head regions reveal no homology to known motor proteins (*21*), and their low ATPase activity is inconsistent with a conventional motor (*12*, *22*). No quantitative measure of their DNA-condensing properties has been previously demonstrated. By extending a single molecule of DNA between two beads within a microchamber (one held in laser tweezers and the other held atop a micropipette), we directly monitored by optical trap microscopy the mechanical activity of purified MukBEF protein on DNA.

The mechanical assay. The mechanical assay is performed by first attaching one end of a 15-kb linear DNA to a polystyrene bead through a biotin-streptavidin linkage (*23*). This construct is held inside a microchamber by a dual-beam optical trap (*24*) and incubated for 1 to 5 min with purified MukBEF in a reaction buffer containing ATP (*25*). The free end of the DNA is then captured via a digoxigenin–antidigoxigenin connection to a second polystyrene bead held atop a pipette by suction (*23*). Moving the pipette bead away from the trap bead at a constant velocity of 300 nm/s increases the distance between the beads and the tension in the DNA. The resulting data can then be displayed by plotting force versus extension.

In the absence of MukBEF, the force-extension curve displays the elasticity of a single torsionally unconstrained DNA molecule with a contour length of 5.1 μm and a persistence length of 50 nm (Fig. 1A, left panel) (*26*, *27*). In contrast, when 12.5 nM MukBEF and 2.0 mM Mg-ATP are added, the force-extension curve rises prematurely, indicating that the tether between the beads has shortened relative to naked DNA (Fig. 1A, right panel). Analysis of this initial part of the curve yields an apparent persistence length of ~21 nm, a value consistent with DNA exposed to MukBEF but not condensed (*23*). At ~17 pN, the tether then undergoes a series of discrete force-extension transitions in a flat sawtooth pattern indicating individual, quantized opening events. When the filament is further stretched (referred to as the final region),

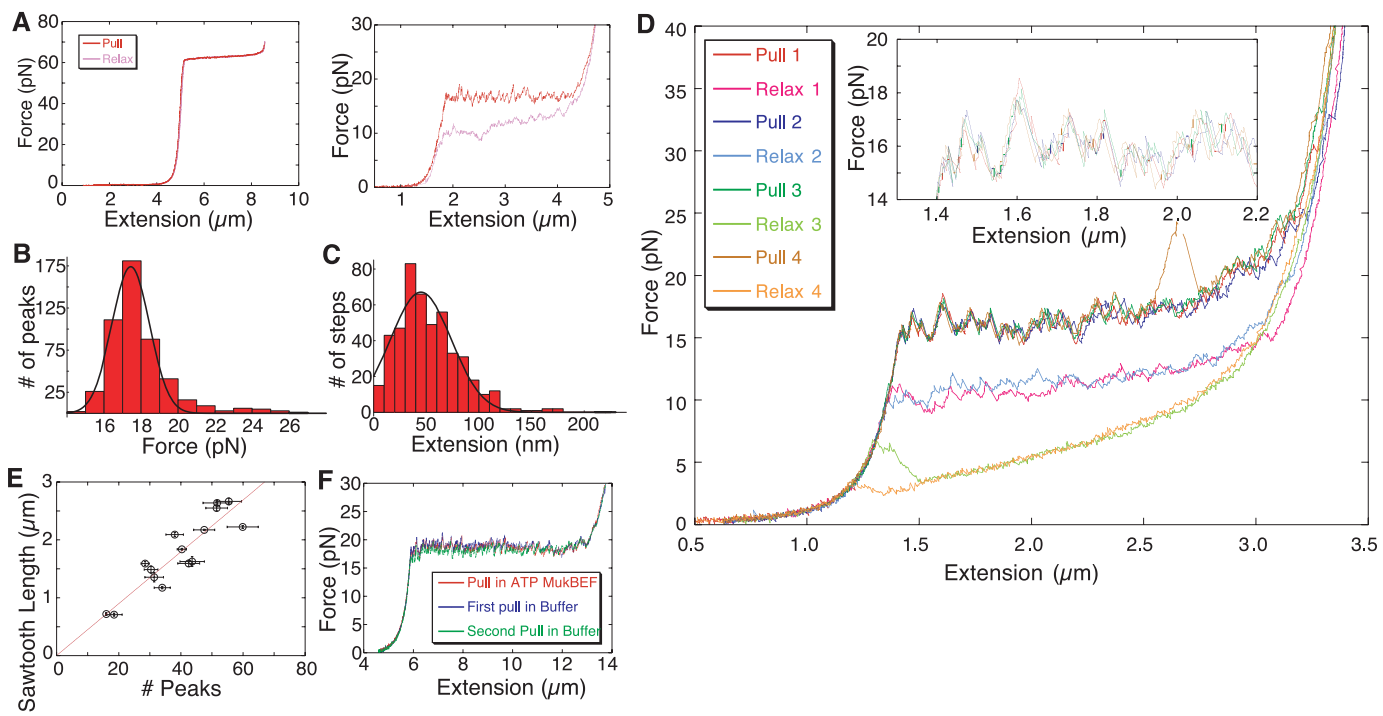

Fig. 1. (**A**) A single force-extension curve of naked DNA (left panel) and DNA after incubation with 12.5 nM MukBEF and 2 mM Mg-ATP (right panel). Pull curves are red; relax curves are pink. There is no hysteresis in the left graph, so the relax curve is hidden underneath the pull curve. (**B**) Peak forces were measured from sawtooth patterns of 15 separate filaments comprising 510 peaks. Fitting the histogram to a Gaussian yields a mean of 17.4 pN (SD = 1.0 pN); 16 points greater than 28 pN were included in the Gaussian fit but are not displayed. (**C**) Step sizes were measured by first fitting the rise of each tooth to an extensible worm-like chain model with a fixed persistence length and stretch modulus and then determining the change in length at 17 pN (*25*). Fifteen separate filaments comprising 480 steps were analyzed to yield a broad distribution that was fit with a Gaussian curve with a mean step size of 45 nm (SD = 29 nm). (**D**) Overlaid force-extension curves for four consecutive pulling/relaxation cycles of a MukBEF-DNA filament demonstrates the high reproducibility of the peaks in a sawtooth pattern (inset). The signature profile is maintained even after some peaks are skipped or a single transition comprising multiple peaks occurs. During subsequent pulling/relaxation cycles, the overlapping or missing transitions disappear and the distinctive sawtooth pattern is restored, hence the aberrant transitions are stochastic and reversible deviations of the structure. (**E**) The number of peaks per length of sawtooth region is plotted for 15 filaments and 111 extension curves. For each filament, multiple pulls were analyzed to give a mean and SD for both the number of peaks and the length of the sawtooth region. The slope of a line fit through the origin gives an average step size of 45 ± 2 nm per peak. The roughly linear relationship demonstrates that although the extent of the DNA bound by MukBEF varies, the filaments are regular without occasional higher order structures or abnormally large loops of DNA. (**F**) Extension and recondensation of a MukBEF filament requires neither free protein nor ATP. Three overlaid force-extension curves for a filament formed using 48 kb of λ DNA, 12.5 nM MukBEF, and 2 mM Mg-ATP are shown. After a pull (red), excess protein and nucleotide were exchanged with buffer and additional pulls were performed (blue and green). The signature pattern remains. For simplicity, only the extension curves are shown.

the force rises sharply in a manner still distinct from that of naked DNA. When a force of 40 pN is reached (*23*), the direction of movement of the pipette bead is reversed and the tension in the tether is lowered, resulting in a relaxation curve that follows a lower force path than does extension (*23*). It is noteworthy that the condensed structure formed when either ATP or the nonhydrolyzable analog adenosine 5′-(β,γ-methylene)triphosphate (AMP-PCP) (*23*) was present, but not when nucleotide was omitted; this finding indicates that the DNA condensation mechanism is an ATP-dependent process that uses energy from nucleotide binding but not from hydrolysis. Presumably, nucleotide binding stabilizes a conformation of the protein complex proficient for condensation.

The sawtooth pattern. The transitions in the flat plateau occur over a narrow force range of 17.4 ± 1.0 pN (Fig. 1B). A histogram of step sizes occurring at ~17 pN revealed a broad peak centered at 45 nm (SD = 29 nm) (Fig. 1C) (*23*). Use of the worm-like chain model to determine the contour length reveals that the DNA released upon extension is 57 ± 38 nm, or ~170 ± 110 base pairs (bp) (*25*). Because the sawtooth pattern spans several micrometers, we conclude that it corresponds to the unraveling of a structure in which every tooth of the pattern corresponds to the extension of a condensation unit—presumably one MukBEF complex and the DNA it engages. The large variation in step sizes likely results from the variable head-to-head distance in MukBEF molecules as they pivot around their central hinge (*28*) before binding DNA. Each complex would thus gather and condense somewhat different lengths of DNA. Analysis of the leading edges of the force peaks and the final region of the force-extension curve yields an extremely short apparent persistence length (~2 nm). This result could be due to protein-induced bending of the DNA or to a continuous change of the contour length of the filament with force. Because the former explanation requires an unrealistically large number of protein-induced bends, it appears more likely that the low apparent persistence length is due to the "peeling" of DNA from the surface of a protein-DNA complex (*25*).

The sawtooth pattern reproduced almost identically over multiple pulling/relaxation cycles (Fig. 1D). This observation indicates that a MukBEF-DNA filament always returns to its original structure at the end of each relaxation cycle; moreover, it implies that individual MukBEFs must remain associated with the same segments of DNA to survive multiple pulling/relaxation cycles. The unexpected high reproducibility of the stretching transitions can be explained if MukBEF proteins associate with DNA to form a single, contiguous structural island. Multiple islands organized in series along the DNA would result in overlapping stretching events and stochastic, nonreproducible sawtooth patterns. The formation of a single structural island requires a highly cooperative organization of MukBEF on DNA, which in turn requires the filament to be stabilized not only by DNA-protein interactions, but also by interactions between neighboring MukBEF molecules. Because the sawtooth patterns are always in the same sequential order, the underlying elements must be released sequentially and unidirectionally from one end. An alternative model in which the order of the peaks is dictated by the strength of interactions would produce a series of peaks ordered by force, with the weakest opening first and the strongest last. Instead, we observe many cases in which peaks of higher force are always followed by peaks of lower force (Fig. 1D, inset).

Each MukBEF-DNA filament, although formed with the same DNA sequence, displayed a unique sawtooth pattern during force-induced extensions (compare Fig. 1A, right panel, and Fig. 1D), implying that the heterogeneity is a result of conformational variability of MukBEF itself. Although the number of peaks in the sawtooth pattern of different filaments varies, the number of peaks is linearly related to the length of the pattern (Fig. 1E). This observation indicates that the structures have a repetitive, possibly periodic nature. The periodicity of the structure derived from the slope of this plot is 45 ± 2 nm per peak, or, within error, the same value obtained from the distribution of step sizes.

These observations show that there are two simultaneous modes of MukBEF binding to DNA. One mode is broken at ~17 pN (see below); the other is insensitive to DNA tension, allowing the protein to remain bound to the DNA at higher forces, and is responsible for maintaining the localization of each MukBEF on the DNA so that the filament returns to the same condensed structure each time after relaxation. One filament formed with a torsionally constrained DNA showed reproducible sawtooth force-extension patterns even after having been briefly held at 90 pN (fig. S1) (*23*).

A filament was assembled and free protein and ATP were washed out of the microchamber with excess buffer. The characteristic repetition in force-extension curves remained even after 20 consecutive pulling/relaxation cycles (Fig. 1F). Therefore, (i) the filament is not at equilibrium with free MukBEF; (ii) the filament is sufficiently stable so that bound MukBEF molecules do not dissociate even at high forces; and (iii) because ATP is not necessary, recondensation must be driven by the interactions that became available between the protein and DNA upon nucleotide binding during filament formation.

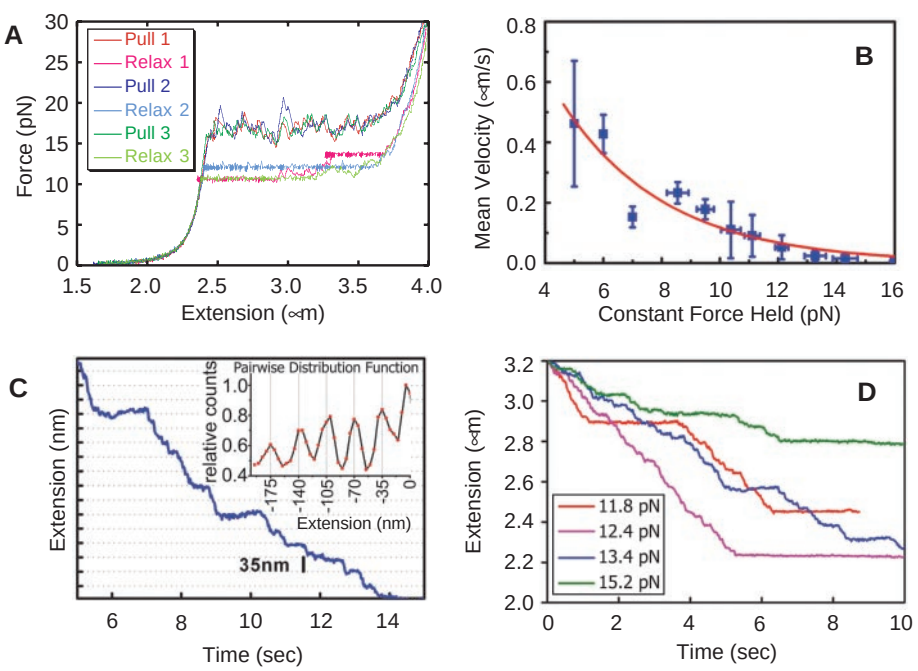

Fig. 2. (**A**) Recondensation against a constant force. If constant-force feedback was used during relaxation (relax 1, 13.6 and 10.5 pN; relax 2, 12.0 pN; relax 3, 10.6 pN), the length of the tether shortened over time, hence the filament could recondense against a force. (**B**) Effect of force on relaxation rate. The force-velocity curves for 53 condensation traces at various constant forces with mean and SD are shown. An Arrhenius analysis was done by fitting the data to an exponential function (red) to obtain a distance of 1 nm from the extended state to the transition state. (**C**) A time trace of a single recondensation experiment at constant force [relax 2 in (A)] shows discrete ~35-nm steps. The histogram (inset) of the corresponding pairwise distribution function clearly shows a periodicity of 35 nm and its multiples. (**D**) Four time traces taken at different constant forces show that recondensation is frequently interrupted with distinct pauses.

Recondensation. If during relaxation the filament is held at a constant force (< 17 pN) using a force feedback mode of the tweezers (*29*), the beads are steadily pulled together as the extended filament recondenses (Fig. 2A). The rate of recondensation diminishes as the force applied to the filament is increased (Fig. 2B), indicating that the rate-limiting step for recondensation is a force-dependent mechanical displacement over the range of forces studied. At constant forces between 12 and 16 pN, the rate of recondensation was sufficiently slow that discrete recondensation steps could be discerned (Fig. 2C). A pairwise distribution function of one recondensation reaction at 12 pN revealed well-resolved 35-nm steps (Fig. 2C, inset). Adding pairwise distribution functions of 21 separate recondensation reactions reveals an average reformation step size of 35 nm (SD = 4 nm) (fig. S2) (*23*). Notably, recondensation occurred in constant-velocity bursts interspersed with distinct pauses (Fig. 2D). The pauses imply that the reformation of the filament also proceeds in a cooperative, sequential manner. If there were instead multiple independent compaction events, distinct pauses would be absent and the recondensation velocity would be expected to be a function of the filament length and to decrease exponentially over time. Cooperative recondensation indicates that even in the extended state, direct protein-protein interactions persist between adjacent MukBEF molecules.

An Arrhenius analysis of the recondensation rate with force yields a distance of only 1 nm from the extended state to the transition state (*23*). The distance from the closed state to the transition state was estimated by dynamic force spectroscopy to be large (at least 20 nm) (*23*). The location of the transition state close to the extended state reveals a "soft" condensed state; that is, the potential energy surface of the condensed state is broad and contains a number of moderately stable intermediate states. Such a soft condensed state could be caused either by elasticity within the protein or by wrapping of the DNA around the protein (see below).

Effect of topoisomerase I. Eukaryotic condensins stabilize DNA supercoils in vitro (*11*, *12*, *15*, *30*), and prokaryotic condensins affect the supercoiling state of the nucleoid in vivo (*31*, *32*). To investigate whether MukBEF also stabilizes DNA supercoils, we repeated pulling/relaxation cycles in the presence of the wheat germ type IB topoisomerase, which relaxes positive and negative supercoils but cannot remove duplex DNA entanglements. Whereas the characteristic sawtooth pattern remained unchanged in the pulling curve, the hysteresis in the relaxation curves almost disappeared (Fig. 3). This experiment was repeated five times with the same outcome. We conclude that in the absence of topoisomerase, the recondensation of the extended filament is slowed down by trapped supercoils (*23*). Topoisomerase eliminates trapped supercoils, leading to filaments that can equilibrate faster between their condensed and extended states, thus reducing hysteresis in the cycle. Because the DNA tether is not torsionally constrained, topological strain must have accumulated in the DNA organized in the filament, possibly in the segments delimited by adjacent MukBEF heads. The MukBEF molecules bound to the DNA thus appear to act as topological domain barriers that anchor the ends of these supercoiled segments and block the transport of torsional stress.

Model. On the basis of these data, we propose a model for the organization of DNA by MukBEF that harmonizes our mechanochemical results with previously published data. According to this model (Fig. 4A), ATP-bound MukBEF molecules polymerize along DNA in a cooperative fashion to form a condensed filament. The length of DNA spanned by the heads of each MukBEF molecule averages ~170 bp but varies because of the flexibility of MukBEF before filament formation. Our results do not indicate whether a tethered or entangled DNA component is part of the mechanism of condensation, although a pure embrace model as proposed for the SMC-family cohesins (*33*) or yeast condensin (*22*) is ruled out.

Two cooperative protein-protein interactions organize the filament. The first involves intermolecular contacts between the heads of adjacent MukBEF molecules along the DNA. We propose that this is the primary ATP-dependent head-head interaction seen in the Rad50 structure (*7*) and that it provides the main protein-DNA contacts that maintain the position of MukBEF molecules along DNA. These head-head and head-DNA interactions are remarkably insensitive to DNA tension and are never broken during the course of our experiments. As a consequence, the filament is able to return to its original conformation, the unique sawtooth pattern is reproducible, and recondensation occurs in a cooperative fashion. These protein-protein interactions constitute a direct demonstration of cooperative interactions in the SMC family.

The second cooperative interaction is force sensitive, involves intramolecular contacts between two heads of the same MukBEF molecule, and makes available protein–nucleic acid contacts involved in DNA condensation. When these interactions are broken by force, MukBEF molecules transition from a closed state to an open state. These ruptures are responsible for the sawtooth pattern at ~17 pN and the concomitant loss of condensation. The contacts of the MukBEF heads to DNA might involve DNA wrapping, such as occurs in nucleosomes that are unwound at 20 to 30 pN (*34*, *35*). It has been reported that DNA wraps twice around a single *Xenopus* 13*S* condensin molecule (*36*).

Because the condensed filament is formed when ATP is replaced by a nonhydrolyzable analog, the energy of nucleotide binding (rather than its hydrolysis) is used to condense DNA. Condensation is mediated by protein–nucleic acid and protein-protein interactions that become available only in the nucleotide-bound form of the protein. The role of ATP in DNA condensation is primarily regulatory, implying that MukBEF condenses DNA by binding stoichiometrically rather than by enzymatic catalysis as in a typical molecular motor.

The sawtooth patterns reproduce almost identically on successive extensions. We therefore conclude that the condensed fiber unravels sequentially from one end. Presumably, a terminal closed-state MukBEF with only a single neighbor is less stable than an interior MukBEF bracketed by neighbors. Therefore, its intramolecular head-head interactions break first under tension. It is unknown whether this is the filament end where nucleation began or the end where polymerization stopped. This first transition destabilizes the closed state of the nearest neighbor, creating a new end element. As a result, extension propagates unidirectionally along the filament.

Because recondensation is cooperative but the path is not reproducible, a nucleation event must first occur somewhere along the extended filament. Then, recondensation propagates cooperatively along the tether, converting MukBEF molecules back to the closed state and reforming the force-sensitive protein-protein and protein-DNA interactions.

The closed configuration of each MukBEF molecule is stabilized by ~530 pN·nm (~15

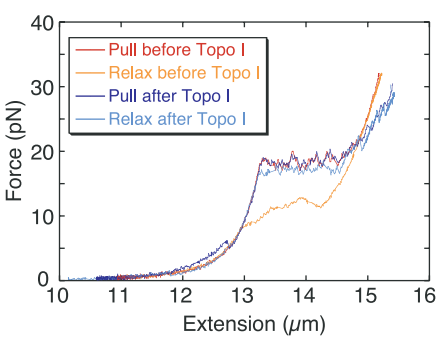

Fig. 3. Enhancement of recondensation by a type I topoisomerase. Shown are two pulling/relaxation cycles from a filament made with λ DNA, 12.5 nM MukBEF, and 2 mM Mg-ATP. Pulling was done at 300 nm/s. The initial pull (red) and relax (orange) curves show the typical hysteresis. After several successive pulling/relaxation cycles, excess MukBEF and ATP were washed out with buffer, and wheat germ topoisomerase I (1 U/ml) was added. Subsequent pulling/relaxation curves obtained in the presence of topoisomerase I (dark blue, light blue) show greatly reduced hysteresis.

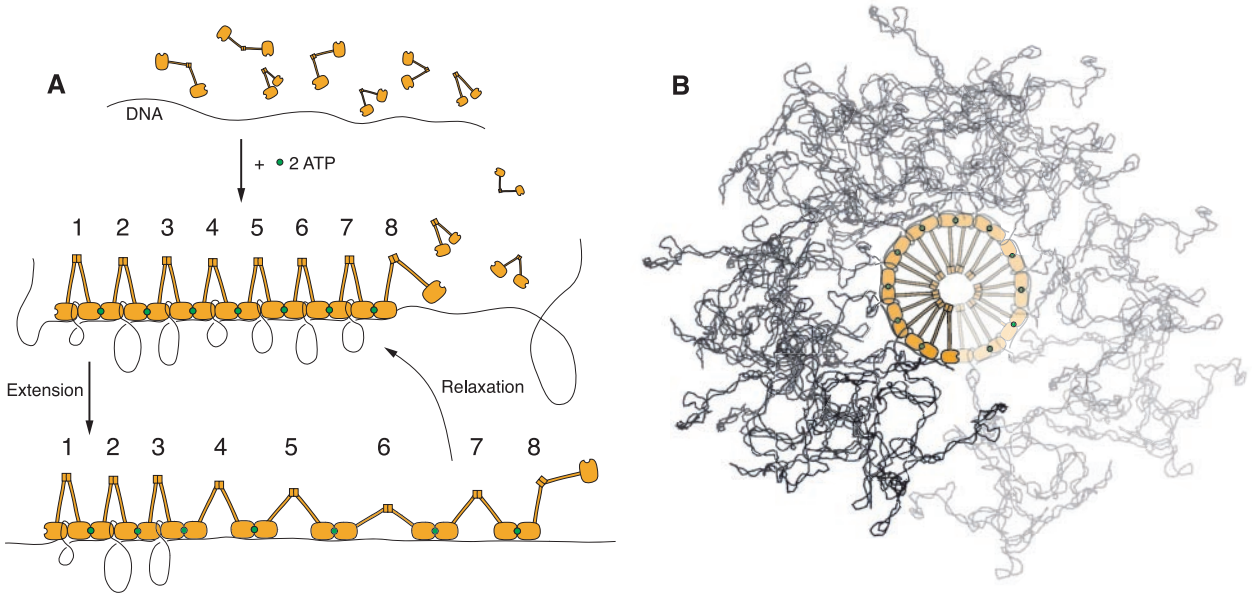

Fig. 4. Model for the DNA condensation mechanism. MukBEF complexes are depicted as orange dumbbell-shaped molecules with a central hinge, DNA as a thin black line, and the two ATPs between adjacent heads as a small green circle. (**A**) Formation, extension, and recondensation of the condensed filament. In an ATP-dependent manner, free MukBEF molecules with various hinge angles cooperatively polymerize along the length of DNA, trapping and supercoiling variable lengths of DNA. The binding propagates along the length of DNA, creating a compact, microheterogeneous, repetitive structure. Intermolecular head-head binding provides force-resistant interactions, whereas intramolecular head-head binding traps DNA in a force-sensitive manner. When the filament is extended, the force-sensitive intramolecular interactions are sequentially broken from one end (7, 6, 5, 4, etc.), releasing variable lengths of sequestered DNA. The contour length of DNA released is ~57 nm, which allows the 100-nm MukBEF to remain bound to the DNA in its extended form, leaving the intermolecular head-head interactions intact. When the force is lowered, recondensation begins with a random nucleation event that cooperatively propagates along the extended filament by reforming the trapped DNA supercoils. Nucleation can occur at different positions along the extended filament, which results in multiple recondensation paths (e.g., 5, 6, 7, 1, 2, 3, 4 and 3, 4, 5, 6, 7, 1, 2). (**B**) A speculative model for condensed DNA in vivo, in which 30-kb loops of supercoiled DNA form topological domains between heads of individual helically propagated MukBEF complexes.

pN × 35 nm) or 80 kcal/mol of binding energy relative to the open configuration. What condensation mechanism could account for this very large energy difference? One possibility is a "Brownian ratchet" mechanism whereby MukBEF heads bound to ~170 bp of DNA are pulled apart by tension, but thermal motion occasionally brings adjacent heads close enough to reform the closed state at forces less than 17 pN. This process will reel in the DNA if the tension falls below this critical value. However, unlike the result for MukBEF, in a Brownian ratchet model the transition state would be located near the closed state. In addition, we calculate that a Brownian ratchet would recondense DNA many orders of magnitude slower than observed (*37*). In a second hypothetical mechanism, the energy for recondensation could arise from the elastic bending of the 50-nm coiled-coil arms. The elastic energy generated from the distortion of the arms away from some preferred angle of the hinge might be transmitted through the arms to pull the DNA together into the closed state. However, coiled coils are more than an order of magnitude too flexible to provide the force needed to condense DNA (*23*). Third, the transition to the open state could cause a partial denaturation of the protein, and the energy of refolding could drive recondensation. This explanation is also unlikely. Because many contacts are lost upon a small deformation of the structure (*38*), mechanical unfolding of protein typically displays transition states very close to the folded state, again contrary to the result for MukBEF. Instead, a transition state close to the open state is consistent with a gradual zipping of two structures that are already in contact, such as occurs in the formation of an RNA hairpin (*29*) and in the wrapping of DNA around histone octamers (*39*). Two processes that could fulfill this role for the MukBEF filament are stepwise reassociation of the coiled-coil arms and winding of DNA around the protein heads. The latter is consistent with the topoisomerase I results showing that MukBEF binds supercoiled DNA, and with the reported wrapping of DNA around a single *Xenopus* 13*S* condensin molecule (*36*).

Conclusion. An important function of condensins is the compaction of DNA. In the case of MukBEF, this process could be brought about by supercoiling between adjacent heads (*11*) and by wrapping around head domains (*36*). From the force-extension transitions observed in this study, we estimate a minimal compaction ratio of ~4 [similar to that found in yeast (*40*)] and a span of ~170 bp of DNA for each MukBEF (*23*). It is possible that the compaction ratio could be much higher if individual MukBEF dimers span nonadjacent segments of DNA. In vivo, there is ~1 MukBEF per ~30 kb of DNA for the entire 4.6-Mbp circular bacterial genome (*41*). Because the nucleoid is already condensed by DNA binding proteins and negative supercoiling (*42*), MukBEF binding sites that are 30 kb apart along the DNA contour may be in close proximity and be trapped between adjacent MukBEF heads. Accordingly, our model for the compact bacterial nucleoid in vivo has long supercoiled regions fixed by MukBEF heads, and the overall structure could adopt a higher order, regular, possibly helical structure in space (Fig. 4B) (*43*). MukBEF would then also be an important contributor to the folding of the chromosome into topological domains. This view would also rationalize the central rather than dispersed location of condensins in chromosomes (*9*, *20*). Finally, the cooperativity seen in vitro would actively promote rapid condensation of DNA in vivo. Our results show that ATP plays a regulatory role for MukBEF condensation, which rationalizes the low observed ATPase rates for condensins. It seems plausible that the rapid decondensation required before DNA synthesis is mediated by ATP hydrolysis or release promoted by exchange factors or chaperones.

References and Notes

1. T. J. Richmond, C. A. Davey, *Nature* **423**, 145 (2003).
2. D. Koshland, A. Strunnikov, *Annu. Rev. Cell Dev. Biol.* **12**, 305 (1996).
3. J. R. Swedlow, T. Hirano, *Mol. Cell* **11**, 557 (2003).

4. D. J. Sherratt, *Science* **301**, 780 (2003).
5. P. L. Graumann, R. Losick, *J. Bacteriol.* **183**, 4052 (2001).
6. C. H. Haering, J. Lowe, A. Hochwagen, K. Nasmyth, *Mol. Cell* **9**, 773 (2002).
7. K. P. Hopfner *et al.*, *Cell* **101**, 789 (2000).
8. M. Yamazoe *et al.*, *EMBO J.* **18**, 5873 (1999).
9. T. Hirano, T. J. Mitchison, *Cell* **79**, 449 (1994).
10. T. Hirano, R. Kobayashi, M. Hirano, *Cell* **89**, 511 (1997).
11. K. Kimura, V. V. Rybenkov, N. J. Crisona, T. Hirano, N. R. Cozzarelli, *Cell* **98**, 239 (1999).
12. K. Kimura, T. Hirano, *Cell* **90**, 625 (1997).
13. A. V. Strunnikov, E. Hogan, D. Koshland, *Genes Dev.* **9**, 587 (1995).
14. T. Sutani *et al.*, *Genes Dev.* **13**, 2271 (1999).
15. K. A. Hagstrom, V. F. Holmes, N. R. Cozzarelli, B. J. Meyer, *Genes Dev.* **16**, 729 (2002).
16. R. A. Britton, D. C. H. Lin, A. D. Grossman, *Genes Dev.* **12**, 1254 (1998).
17. H. Niki, A. Jaffe, R. Imamura, T. Ogura, S. Hiraga, *EMBO J.* **10**, 183 (1991).
18. T. Weitao, K. Nordstrom, S. Dasgupta, *Mol. Microbiol.* **34**, 157 (1999).
19. J. A. Sawitzke, S. Austin, *Proc. Natl. Acad. Sci. U.S.A.* **97**, 1671 (2000).
20. K. Ohsumi, M. Yamazoe, S. Hiraga, *Mol. Microbiol.* **40**, 835 (2001).
21. F. van den Ent, A. Lockhart, J. Kendrick-Jones, J. Lowe, *Structure Fold. Des.* **7**, 1181 (1999).
22. J. E. Stray, J. E. Lindsley, *J. Biol. Chem.* **278**, 26238 (2003).
23. See notes S1 to S14 in SOM Text at *Science* Online.
24. S. B. Smith, Y. Cui, C. Bustamante, *Methods Enzymol.* **361**, 134 (2003).
25. See supporting data at *Science* Online.
26. S. B. Smith, Y. Cui, C. Bustamante, *Science* **271**, 795 (1996).
27. S. B. Smith, L. Finzi, C. Bustamante, *Science* **258**, 1122 (1992).
28. T. E. Melby, C. N. Ciampaglio, G. Briscoe, H. P. Erickson, *J. Cell Biol.* **142**, 1595 (1998).
29. J. Liphardt, B. Onoa, S. B. Smith, I. Tinoco, C. Bustamante, *Science* **292**, 733 (2001).
30. K. Kimura, O. Cuvier, T. Hirano, *J. Biol. Chem.* **276**, 5417 (2001).
31. T. Weitao, K. Nordstrom, S. Dasgupta, *EMBO Rep.* **1**, 494 (2000).
32. J. C. Lindow, R. A. Britton, A. D. Grossman, *J. Bacteriol.* **184**, 5317 (2002).
33. S. Gruber, C. H. Haering, K. Nasmyth, *Cell* **112**, 765 (2003).
34. Y. Cui, C. Bustamante, *Proc. Natl. Acad. Sci. U.S.A.* **97**, 127 (2000).
35. B. D. Brower-Toland *et al.*, *Proc. Natl. Acad. Sci. U.S.A.* **99**, 1960 (2002).
36. D. P. Bazett-Jones, K. Kimura, T. Hirano, *Mol. Cell* **9**, 1183 (2002).
37. J. Howard, *Mechanics of Motor Proteins and the Cytoskeleton* (Sinauer Associates, Sunderland, MA, 2001), pp. 61–63.
38. C. Bustamante, Y. R. Chemla, N. R. Forde, D. Izhaky, *Annu. Rev. Biochem.*, in press.
39. J. D. Anderson, A. Thastrom, J. Widom, *Mol. Cell. Biol.* **22**, 7147 (2002).
40. V. Guacci, E. Hogan, D. Koshland, *J. Cell Biol.* **125**, 517 (1994).
41. M. Kido *et al.*, *J. Bacteriol.* **178**, 3917 (1996).
42. N. R. Trun, J. F. Marko, *ASM News* **64**, 276 (1998).
43. C. D. Hardy, N. J. Crisona, M. D. Stone, N. R. Cozzarelli, *Philos. Trans. R. Soc. London Ser. B* **359**, 39 (2004).

44. We thank V. V. Rybenkov for providing the MukBEF-10xHis plasmid, E. Watson for protein purification, R. Fezzie for scientific discussions, and N. Forde, D. Izhaky, J. Choy, Z. Bryant, C. Cecconi, and J. Stray for critical review of the manuscript. Supported by a Life Science Research Foundation Burroughs Wellcome Fellowship (R.B.C.), a Soong Fellowship (Y-P.C.), the Fannie and John Hertz Foundation (J.G.), NIH grants GM32543 (C.B.) and GM31655 (N.R.C.), and U.S. Department of Energy grants DE-AC03-76DF00098 (C.B.), GTL2BN "Microscopies of Molecular Machines" (C.B.), and SNANOB "Design of Autonomous Nanobots" (C.B.).

Supporting Online Material
www.sciencemag.org/cgi/content/full/1098225/DC1
Materials and Methods
SOM Text
Figs. S1 to S5
References and Notes

23 March 2004; accepted 20 May 2004
Published online 3 June 2004;
10.1126/science.1098225
Include this information when citing this paper.

REPORTS

Control of Light Emission by 3D Photonic Crystals

Shinpei Ogawa, Masahiro Imada, Susumu Yoshimoto, Makoto Okano, Susumu Noda*

Three-dimensional (3D) photonic crystals containing artificial point defects have been fabricated to emit light at optical communications wavelengths. They were constructed by stacking 0.7-micrometer-period gallium arsenide striped layers, resulting in a 3D "woodpile" photonic crystal. Indium–gallium arsenide–phosphide quantum-well layers emitting at a wavelength of 1.55 micrometers were incorporated in the center of the crystal. Samples having up to nine stacked layers were constructed, and artificial point-defect cavities of different sizes were formed in the light-emitting layer. Light emission was suppressed in the photonic crystal regions, whereas cavity modes were successfully observed at the point defects and were size dependent.

Much interest has arisen in photonic crystals (PCs) (*1*–*20*), in which the refractive index changes periodically. A photonic band gap (PBG) is formed in the crystals, so that the propagation of electromagnetic waves is prohibited within the PBG for all wave vectors. These materials are becoming a powerful tool for the manipulation of photons with the aid of artificially introduced defects and/or light emitters. Although progress has been made in creating two-dimensional (2D) PCs (*4*–*14*), revealing the feasibility of their application to devices, there is also increasing interest in 3D PCs (*3*, *15*–*20*). For example, demonstrations of physically interesting phenomena, such as the suppression and/or enhancement of light emission, have been pursued (*1*, *17*–*20*) from the initial stages of PC research. The construction of highly functional integrated photonic chips and the application of the properties of a PBG to optical quantum information processing also require 3D PCs. For all of these applications, 3D PCs with a full PBG should be constructed to satisfy their demanding requirements. It must be possible to introduce an arbitrary defect state into the crystal at any position, as well as to incorporate an efficient light-emitting element. We have succeeded in creating full 3D PBG crystals operating at near-infrared wavelengths (*3*) by means of advanced wafer-fusion tech-

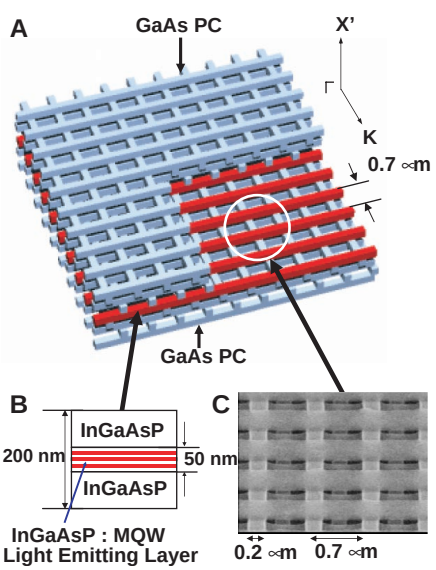

Fig. 1. The 3D PC developed in this study. (**A**) Schematic structure of the 3D active-layer PC developed in this work. (**B**) Structure of the InGaAsP MQW introduced as the light-emitting region in the center of nine layers. (**C**) Scanning electron microscope (SEM) image of the MQW and underneath the GaAs PC layers.

Department of Electronic Science and Engineering, Kyoto University, Kyoto 615–8510, Japan.

*To whom correspondence should be addressed. E-mail: snoda@kuee.kyoto-u.ac.jp